Stiff morphing composite beams inspired from fish fins

Saurabh Das[a], Prashant Kunjam[a], Baptiste Moling[a,b], Tian Gao[a], and Francois Barthelat[a]*

[a] Department of Mechanical Engineering, University of Colorado, 427 UCB, 1111

Engineering Dr, Boulder, CO 80309, USA

[b] Ecole Polytechnique, Route de Saclay, 91128 Palaiseau, France

* Correspondence to: francois.barthelat@colorado.edu

Abstract

Morphing materials are typically either very compliant to achieve large shape changes, or very stiff but with small shape changes that require large actuation forces. Interestingly fish fins overcome these limitations: Fish do not contain muscles, yet they can change the shape of their fins with high precision and speed while producing large hydrodynamics forces without collapsing. Here we present a "stiff" morphing beam inspired from the individual rays in natural fish fins. These synthetic rays are made of PMMA outer beams ("hemitrichs") connected with rubber ligaments which are 3-4 orders of magnitude more compliant. Combinations of experiments and models show strong nonlinear geometrical effects in these synthetic rays: The ligaments are "mechanically invisible" at small deformations, but they delay buckling and improve the stability of the ray at large deformations. We used the models and experiments to explore designs with variable ligament densities, and we generated design guidelines for optimum morphing shape (captured using the first moment of curvature), and that capture trade-offs between morphing compliance (ease of morphing the structure) and flexural stiffness. The design guidelines proposed

here can help the development of stiff morphing bioinspired structures for a variety of applications in aerospace, biomedicine, or robotics.

Keywords: Bioinspiration, fish fins, shape morphing, architected materials, soft robotics

I) Introduction

Morphing refers to radical shape changes in materials and structures [1] which involve large amplitudes and/or unusual deformation modes such as auxetics [2], or the coupling of deformation modes such as compression-induced twist [3]. When a change of geometry is needed in an engineering system, morphing materials offer more advantages than traditional discrete mechanisms: lighter weight, smoother transitions, better distributed stresses, simpler kinematics, smaller numbers of actuators, higher reliability. A wide range of technologies are available for engineering morphing materials: metamaterials [4]–[6], origami [7], kirigami [8], hydrogels [9], hygromorphs [10], pneumatic shape-morphing elastomers [11], [12]. Radical shape change is achieved in these materials, but only with relatively soft materials and structures that cannot sustain large external forces without excess deformations, collapse or failure. Much stiffer and stronger structures can also be morphed using piezoelectric actuators [13] or shape memory alloys [14], but they require large actuation forces that result in only relatively small morphing amplitudes. This conflict between "morphing efficiency" and stiffness from external loads, illustrated on figure 1a, has been a major obstacle to the systematic use of morphing materials in aerospace and other domains [15]. Other design strategies have been proposed for morphing structures, with interesting combinations of stiffness and morphing. However, these structures rely on complex structures found by topology optimization [16], local instabilities [17] or multi-part mechanisms with

actuation that must be transmitted through the entire structure, involving pulleys [18], sliding elements [19], shafts [20] or pneumatics [21] covered by flexural skin, or complicated architected materials made of hundreds of moving parts [20], [22]. Interestingly, fish fins from ray-finned fishes (Actinopterygii) seem to overcome these limitations. Fish fins do not contain muscles but display large morphing amplitudes, combined with high stiffness from external loads (hydrodynamic forces), fast response times and actuation from the base only. Fish fins "probably represents the most elaborate and refined adaptation to efficient interaction with water that has ever evolved" [23] and as such, they can serve as models for the design of new morphing materials. Because they contain no muscles, fish fins are often thought of as passive swimming surfaces which are simply "flapped" for propulsion or passive stabilization. Fish fins are in fact much more sophisticated systems: Fish can adjust not only the orientation, but also the curvature, shape, and surface of their fins to finely tune hydrodynamic interactions and to generate powerful forces in three dimensions [24] (Fig. 1b,c). Individual fish fins are composed of a collagenous membrane stiffened by 10-30 beam-like structures called rays. Each ray has a diameter in the order of ~100 μm with a tapered profile and aspect ratio > 100 (Fig. 1d-f). The rays are composed of two bony layers called hemitrichs which are connected by collagen fibrils embedded in ground gel-like substance (Fig 1f).
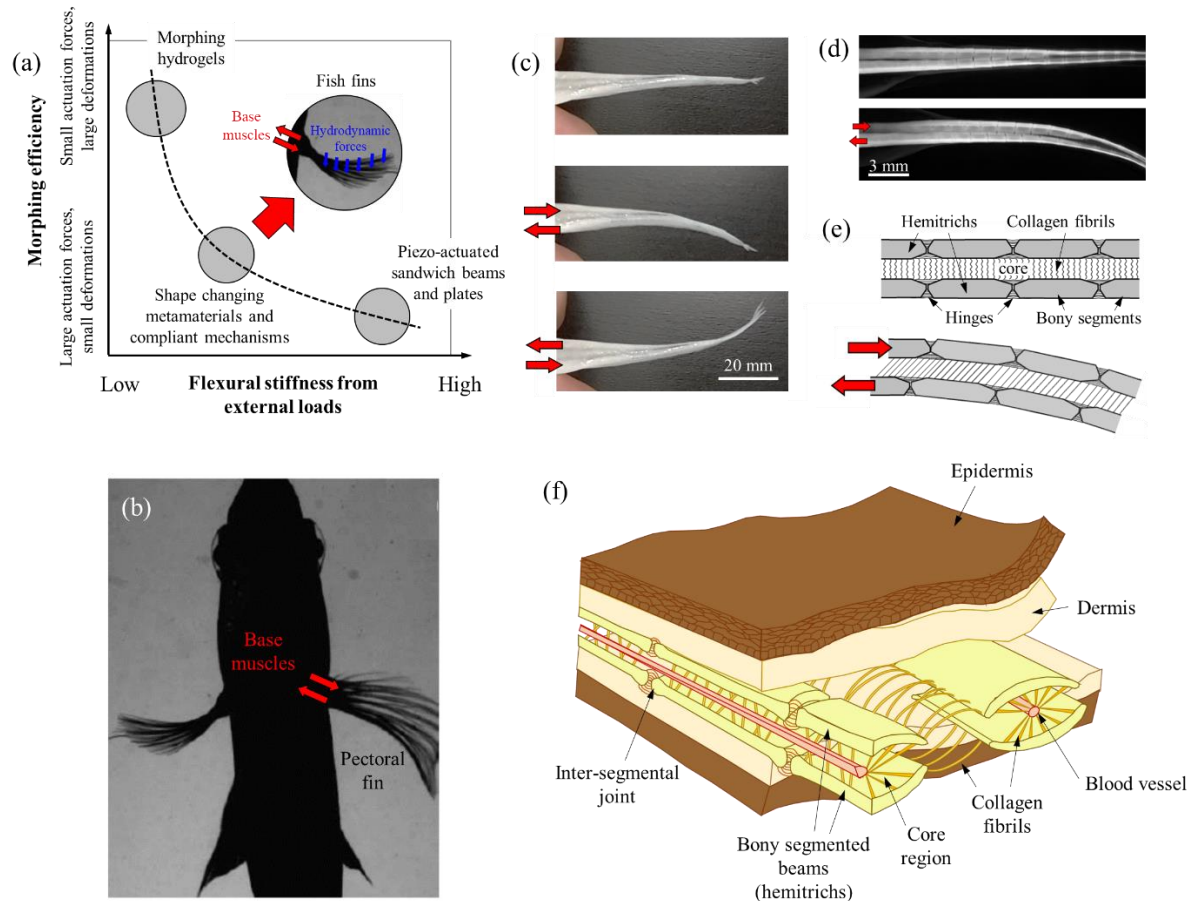
Figure 1: Key features in individual fin rays: (a) Fish fins combine high morphing efficiency and high stiffness from external loads, two properties that are mutually exclusive in engineering morphing materials. (b) Fish can change the shape and effective surface of their fins from actuation by base muscles (Adapted from [24]) (c) An individual ray from a fish fin harvested from Atlantic salmon (*Salmo salar*) is "morphed" by applying push/pull forces manually; (d) MicroCT scans of a caudal fin ray from Atlantic salmon in rest position and actuated position. The hemitrichs "glide" on one another, which induces flexural deformations; (e) schematic of this mechanism; (f) Cross section of a fin showing the bony rays and surrounding softer tissues.

A remarkable feature of fish fins is that their curvature can be adjusted solely by muscular actuation from the base of the rays (Fig. 1b). Push/pull actuation induces shear deformations in the core region, while rotations at the base are prevented by the configuration of the tendons and by a cartilaginous pad at the base of the fin. The shear deformation imposed at the base induces competition between flexural deformation of the hemitrichs and the shear deformation of the core,

over a length scale governed by mechanics. For proper morphing, this "morphing length" must match the length of the fin and there is a fine balance between the flexural stiffness of the hemitrichs and the shear stiffness of the core, so that individual rays can morph along their entire length [25]. Individual rays must also be stiff to minimize deformations and prevent collapse when subjected to hydrodynamic loads. Flexural experiments on individual rays have indeed revealed relatively high flexural stiffness, with homogenized flexural modulus in the order of 1 GPa [26] (for comparison, synthetic materials with large morphing amplitudes are orders of magnitude softer). We have recently measured and modeled the morphing and flexural stiffness performance of individual rays from rainbow trout (*Oncorhynchus mykiss*) [27]. We found that the collagenous core region is best modeled with spring elements, and that these elements are 3-4 orders of magnitude more compliant than the hemitrichs. We also showed that to properly capture the large deformations and large rotations of natural rays, linear models used previously for fins [24], [25], [28]–[30] are not adequate, and numerical models that capture geometrical nonlinearities are needed. Fish fins represent an elegant, robust and mechanically efficient solution to stiff morphing, and they have already inspired a multitude of morphing structures: 3D printed segmented composites [28], flexible fish-like robotic systems [31]–[37], aquatic-aerial vehicles or robots [38]–[40], bioinspired morphing fins as propulsors and to improve maneuverability for autonomous underwater vehicles (AUVs) [41]–[48]. Fish fins have also inspired a variety of robotic gripper designs [49]–[53]. However, among these fish-inspired structures, few truly duplicate the mechanisms of morphing of the natural rays. For example, a majority of fin-inspired robots simply rely on passive, flexural membranes. A thorough understanding of the interplay of soft and hard elements at regimes of large deformations and large rotation is still needed. Here we propose a new design for a fin-inspired stiff morphing beam that captures the main features of

natural rays: stiff outer hemitrich connected by compliant ligaments, morphing with large deformations and large rotations. The mechanics of morphing and flexural deflection of this system are explored using a combination of mechanical experiments and non-linear finite element models, which leads to design guidelines for fin ray-inspired morphing beams.

II) Synthetic fin ray design and fabrication

The objective of the synthetic fin ray was to capture some of the main features of natural fin rays: (i) a slender and slightly tapered overall geometry, (ii) a pair of hemitrichs connected with ligaments, (iii) Hemitrichs at least three orders of magnitude stiffer than the ligamentous core region. Figure 2 shows a design that captured these key features. The overall dimensions of the ray ($L = 200$ mm by $h_0 = 20$ mm by $w = 5$ mm) and the taper angle ($\theta = 5°$) were maintained constant throughout this study, to focus on the effects of the relative properties of hemitrichs and core region. The outer hemitrichs were made from 1.5 mm thick polymethyl methacrylate sheets (PMMA, US Plastic, OH, USA). PMMA is a relatively stiff polymer, with a measured flexural modulus $E_h = 2.8$ GPa. Each hemitrich is a $t_h = 1.5$ mm thick and $w = 5$ mm wide beam, with a wider region at the base for attachment to our mechanical testing platform. To duplicate the softer collagenous core in natural rays we used 1.6 mm thick rubber sheets (RubberCal, CA, USA). The collagenous core in natural rays has a fibrillar structure, with collagen fibrils aligned perpendicularly to the axis of the ray (Figure 1b), a fibrillar arrangement with important implications for the mechanical performance of the ray. To duplicate this structure, we used rubber in the form of ligaments (Figure 2). For this study we maintained the cross-section of the individual ligament constant (1.6 mm by 1.6 mm), but we varied their spacing d (Figure 2) as a way to manipulate the effective elastic properties of the core region. The rubber has a measured tensile

modulus of E_r = 1.52 MPa (measured using tensile tests). The homogenized, effective tensile modulus E_c of the core was calculated using:

$$E_c = \frac{E_r A_r}{dw}$$ (1)

where E_r is the tensile modulus of rubber (E_r = 1.52 MPa), A_r is the cross-section of individual rubber ligaments (A_r = 2.56 mm^2) and w is the width of the hemitrich (w = 5 mm). The distance d between the ligaments was varied from 1.6 mm to 16.6 mm, resulting in an effective tensile modulus of the core region E_c in the 50 to 500 kPa range. The contrast in elastic properties between the PMMA hemitrichs and the ligamentous rubber core was therefore more than three orders of magnitude, in consistence with measurement on natural fin rays [27].
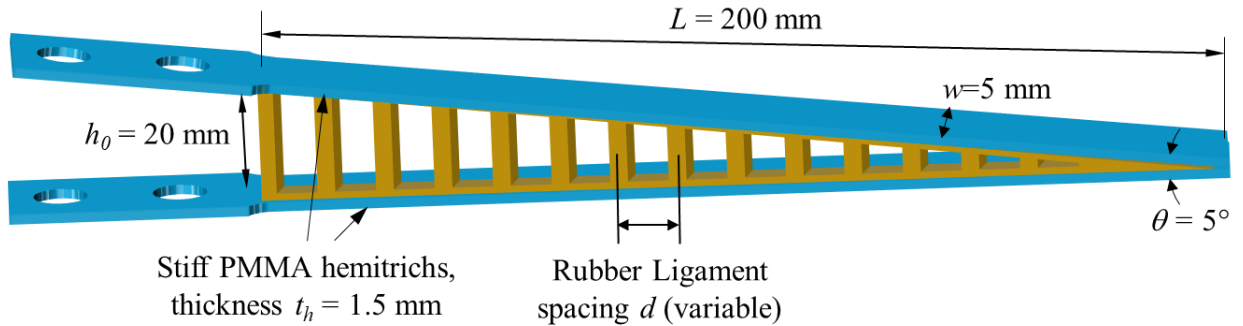

Figure 2: Overview of the design and geometry for the synthetic ray

Fabrication started with the pre-conditioning of the rubber sheets by manual stretching for about 10 cycles. The hemitrichs and rubber ligaments were then cut from sheets using a 80W CO2 precision laser cutter (Nova35, Thunder Laser Systems, TX, USA). Laser cutting produced components with high dimensional fidelity, and we verified that the dimensions of the laser cut components (hemitrich width, rubber ligaments cross section and spacing) were as specified and repeatable using an optical microscope (Leica DM2700 M). The two hemitrichs were glued together at the tip using cyanoacrylate, using 5° wedges to accurately control the taper angle of the

ray. The rubber ligamentous core was then glued to the inner surfaces of the two hemitrichs using cyanoacrylate and the fin ray was then allowed to cure for at least 24 hours. Using this fabrication procedure, we fabricated fin rays with nine different ligament spacings ranging from $d = 1.6$ mm to $d = 16.6$ mm, corresponding to ligament densities of about 180 to 630 ligaments /m (Figure 3a-c). We also fabricated three "extreme" designs: A "Coreless" designs with no ligaments (Figure 3d), a ray entirely made of rubber (Figure 3e) and a ray entirely made of PMMA (Figure 3f).
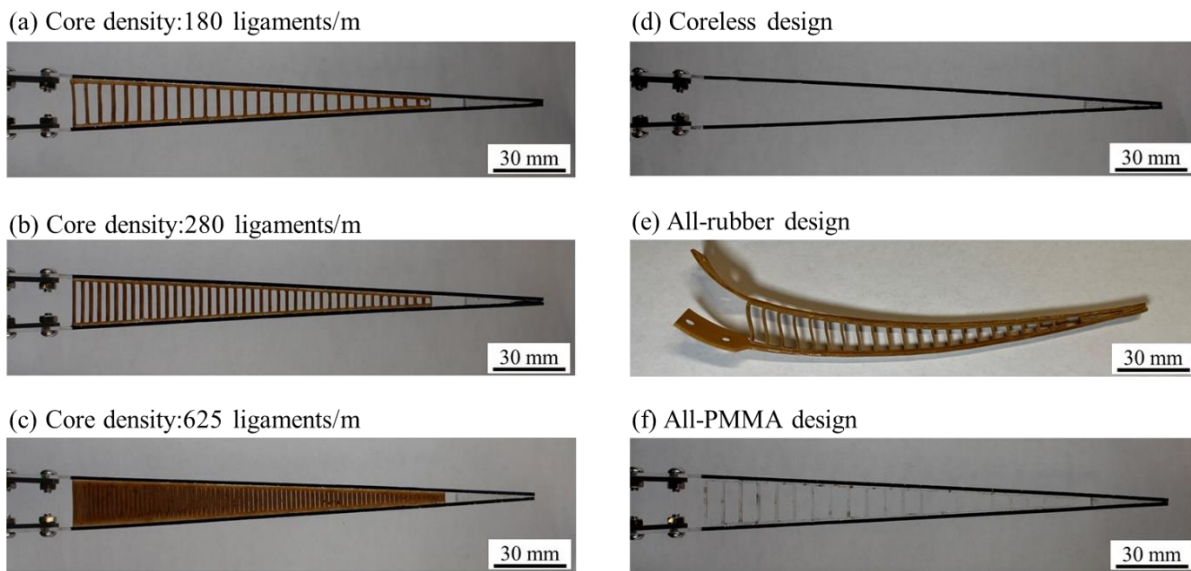

Figure 3: Examples of synthetic fin rays: (a-c) Fin rays with ligaments of increasing density; (d) coreless fin ray (i.e. no ligaments connect the hemitrichs); (e) an "all-rubber" design and (f) "all-PMMA" design.

II) Mechanical testing

The synthetic rays were tested using the micromechanical testing platform shown on figure 4. The upper hemitrich was clamped to the base of the setup, while the lower hemitrich was clamped in line with a motorized micromanipulator (SOLO Single Axis Manipulator Controller, Sutter Instrument, CA, USA). The first type of test was the morphing test, where the lower transducer imposed a displacement u_0 on the base of the lower hemitrich, while the resulting actuation force

F_0 was recorded with a precision load cell (REB7 Subminiature Load Cell, 5 kg capacity, Loadstar Sensors) mounted in line with the transducer. The second type of test was the flexural test, where both hemitrichs were clamped. A transverse displacement δ was imposed at a distance $L_s = 130$ mm from the base, and the corresponding transverse force P was recorded with a precision load cell mounted in line with the transducer. For both tests, optical images of the ray were automatically acquired at regular intervals using a digital camera (Canon EOS Rebel T6). The control of the transducers, the acquisition of the forces, and the acquisition of the pictures were all managed with an interface and a unified custom Matlab code. The morphing and flexural tests were non-destructive, so each ray could be tested multiple times in either morphing or flexural configuration, with highly repeatable results. At the post-processing stage, the images were analyzed using a custom Matlab code to track the position of the hemitrich and digitally reconstruct the deformed shape ("elastica"). To this end, the sides of the hemitrichs were painted in black.
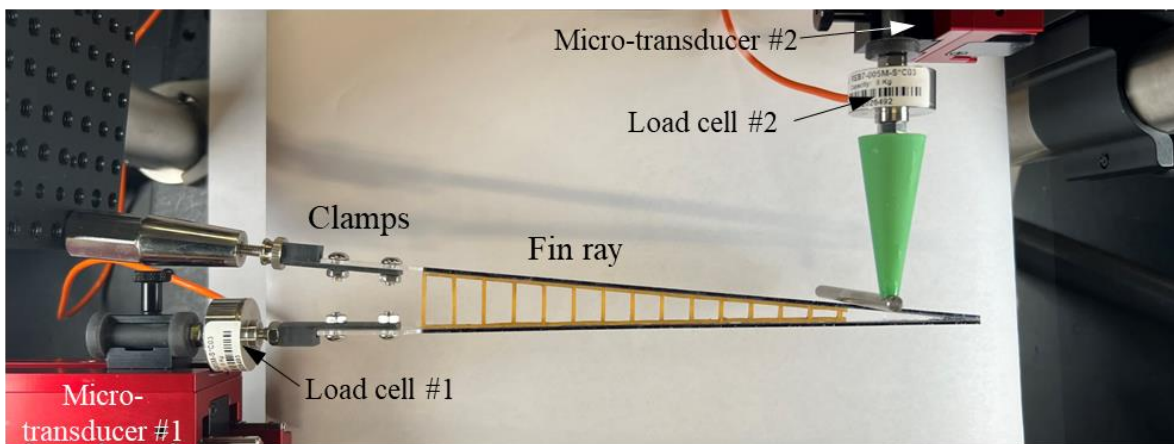

Figure 4: Experimental platform used for the morphing test and for the flexural test on synthetic fin rays.

Figure 5 shows typical results from morphing tests on a fin ray with a ligament spacing $d = 7.6$ mm, shown together with results from a "coreless" ray for reference (i.e. no ligaments). At small deformations, both designs display the same mechanical response, because the rubber ligaments,

initially perpendicular to the hemitrichs, produce little resistance to morphing (they are "mechanically invisible"). At larger deformations, however, there are pronounced differences between the responses of these two designs. The coreless design shows evidence of buckling of the lower hemitrich (which carried a compressive force), accompanied with softening on the F_0-u_0 curve, while the design with ligaments shows stiffening and a much more stable response.
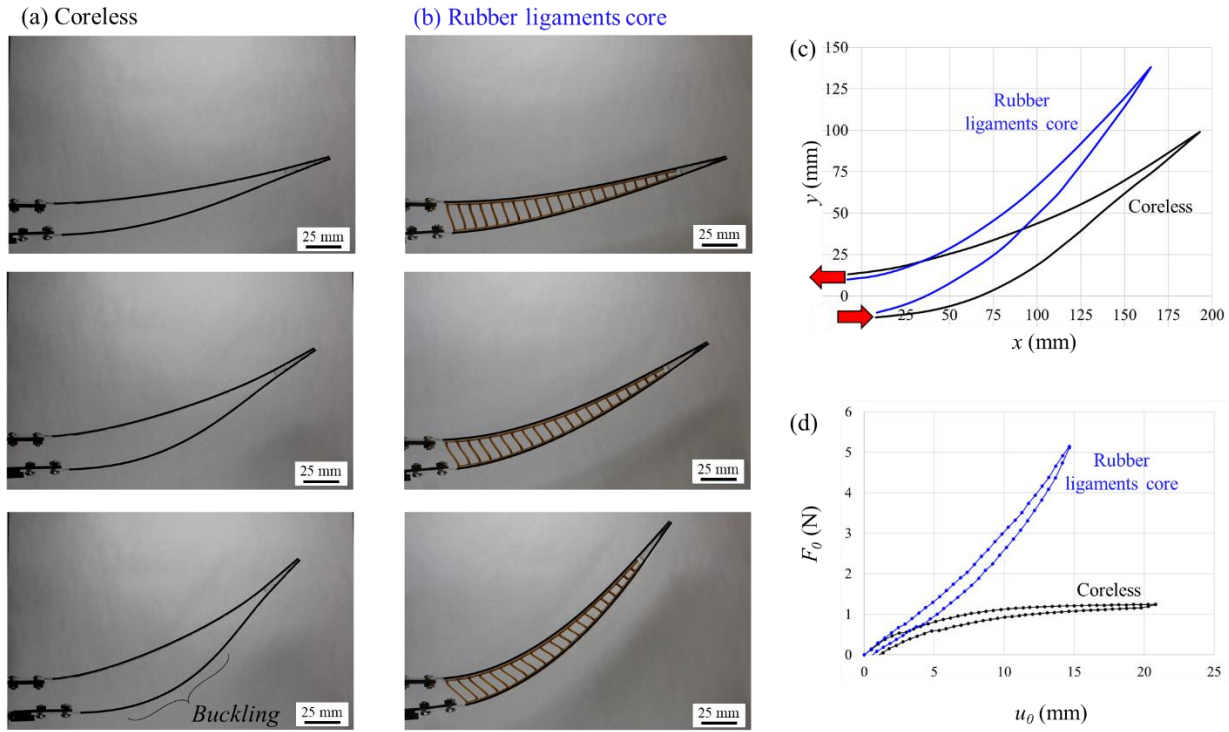

Figure 5: Typical results from morphing experiments: Snapshot of morphed rays for (a) coreless and (b) rays with rubber ligament cores (130 ligaments/m); (c) comparison of morphed profiles (elastica); (d) Actuation force-displacement (F_0-u_0) curves.

Figure 6 shows typical results from the cantilever test on the same two rays. Here again, the two designs produce identical mechanical responses at small deformations, where the contribution of the rubber ligament to overall stiffness is negligible. At larger deformations, the coreless design again shows evidence of buckling, while the design with a core displays a more stable mechanical response and sustained stiffness. These results highlight an important function of the ligaments:

10

The ligaments are mechanically "invisible" at small deformations, which is beneficial because it decreases the actuation force required to initiate morphing from the straight configuration. At large deformation however, the ligaments rotate and stretch, stiffening the entire structure. Importantly, they keep the hemitrichs together at large deformations, which increases the actuation force but also delays the buckling of the hemitrichs. The ligaments also enable a more thorough morphing of the ray in terms of deformation and kinematics. We finally note that while all curves presented here show an elastic response where the initial shape of the ray was recovered upon removal of the load, there is also a small amount of hysteresis from viscous dissipation in the rubber ligaments.
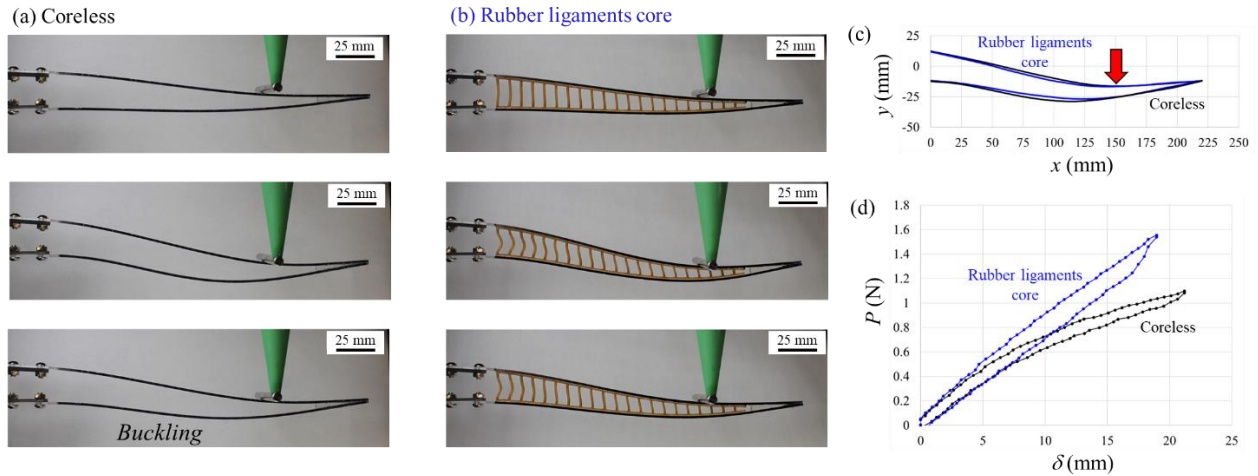

Figure 6: Typical results from flexural experiments: Snapshot of deflected rays for (a) coreless and (b) rays with rubber ligament cores (130 ligaments/m); (c) comparison of elastica; (d) Transverse force-displacement (P-δ) curves.

Finite element model and design exploration

In order to model and optimize the mechanics of the ray, we developed non-linear finite element models that captures large deformations and large rotations [27] (Fig. 7). The hemitrichs were modeled with elastic co-rotational beam elements, with all stiffnesses derived from the modulus of PMMA and the cross-sectional dimensions of the hemitrichs. In the model these elements

11

predominantly deformed in flexion. The rubber ligaments were modeled explicitly, using their cross section and the modulus of rubber. These elements predominantly deformed in tension, although some bending was also observed.
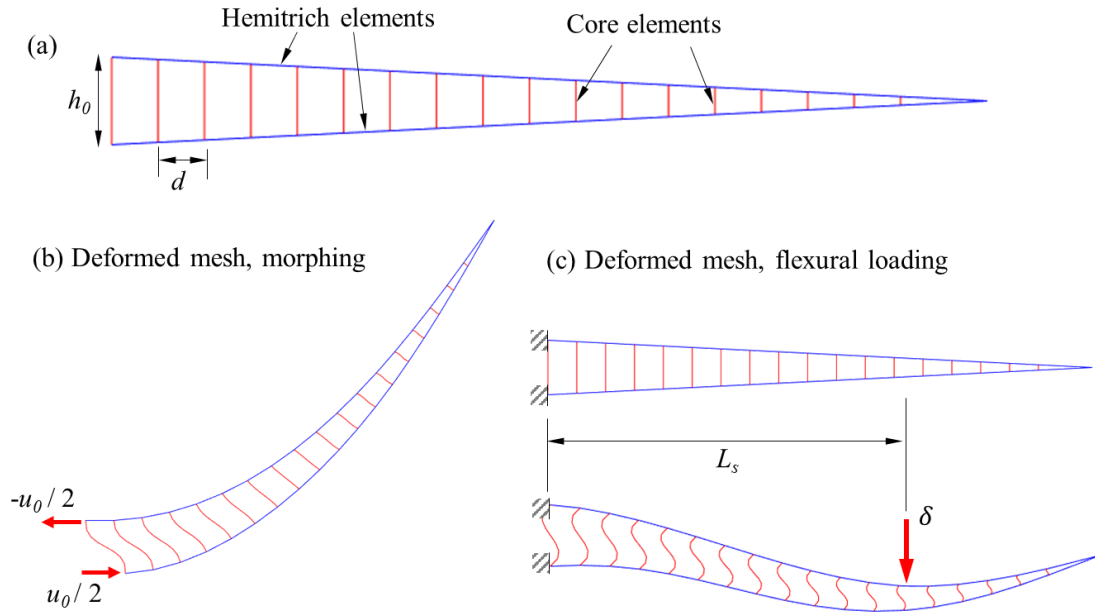

Figure 7: Non-linear finite element model: (a) Mesh with nonlinear corotational beam element: stiff blue elements for the hemitrich, and softer red elements for the ligaments; boundary conditions and typical deformed shapes for (b) morphing and (c) flexural loading

Figure 8 shows comparisons between the model predictions and the experiments. There are good agreements between experiments and models for the morphing and flexural loading configurations, in terms of both elastica and force-displacement curves. This model, therefore, provides a robust and computationally efficient approach to modeling the ray-like beam at large deformations.
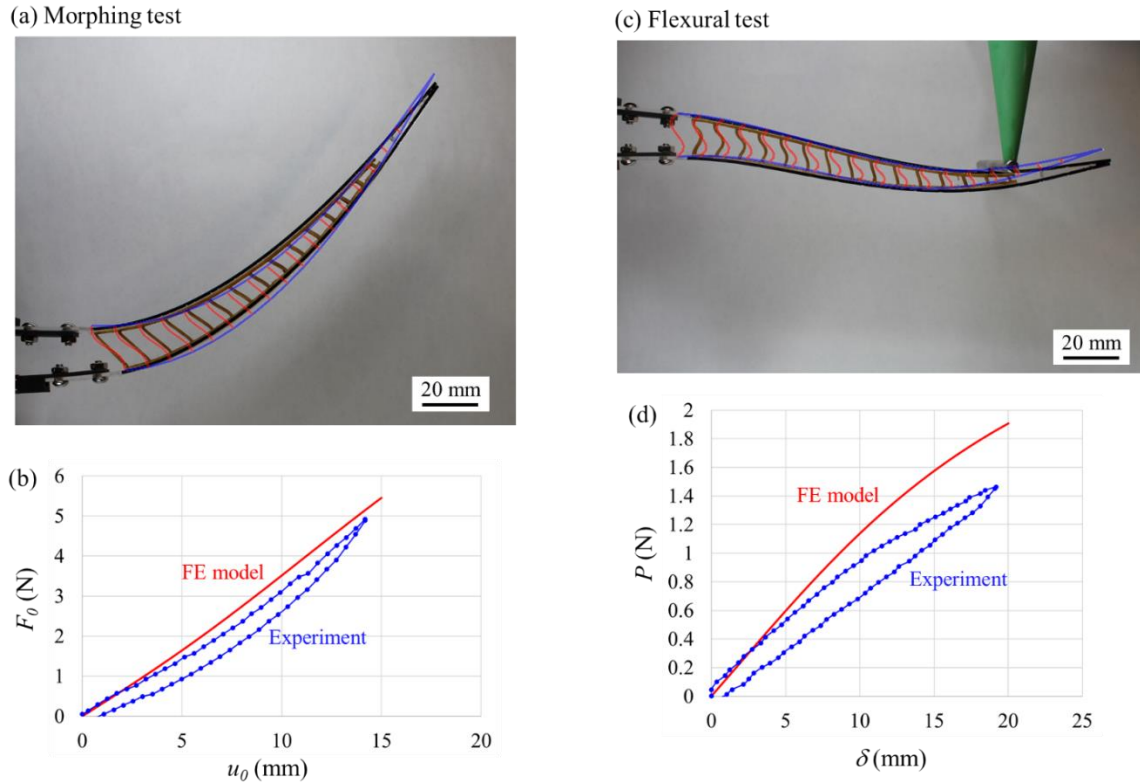
12

Figure 8: Comparison between experiments and models: (a) Elastica and (b) F_0-u_0 curves from pure morphing test; (c) Elastica and (d) P-δ curves from the flexural test.

The design of this bioinspired morphing structure has many variables, which can be tuned and optimized using the models and experiments described above. However, it is important to first define what constitutes a "good design" for this structure. For this study we used three performance metrics: the morphing curvature, which captured whether the deformation due to morphing propagated along the entire ray, the morphing compliance which captured how much "actuation" force is needed to morph the ray, and the flexural stiffness which characterized the stiffness of the structure when subjected to an external transverse force. These three metrics are described in more details in the following sections.

Morphing curvature: When subjected to actuations at the base, the curvature of natural fin rays is distributed almost over their entire length, in other words, fish can manipulate not only the

orientation but also the shape of their fins solely from muscular push-pull at the base of the fins. Our morphing experiments on the synthetic fins produced a similar response, but to various extents. An important measure of the morphing shape in this configuration is the local curvature of the ray $\kappa(s)$, where s is the curvilinear position from the base of the ray. We measured $\kappa(s)$ from the experiments using in-situ images, or from the model using the nodal positions, using the Pratt method [54]. Figure 9 shows two plots of $\kappa(s)$, normalized by h_0, as function of the curvilinear distance s from the base (also normalized by h_0). In one of the designs the density of ligaments is high, which produces a stiff core region and a curvature concentrated near the base (Figure 9). This type of response may be described as a deformation hinge near the base of the ray, while the rest of the ray rotates but remains undeformed. In the second case, the density of ligaments is lower, which produces a more compliant core region and a morphing response which is well distributed over the entire length of the ray. In terms of morphing, the second case is preferable, but a metric is needed to quantitatively rank and optimize different designs.
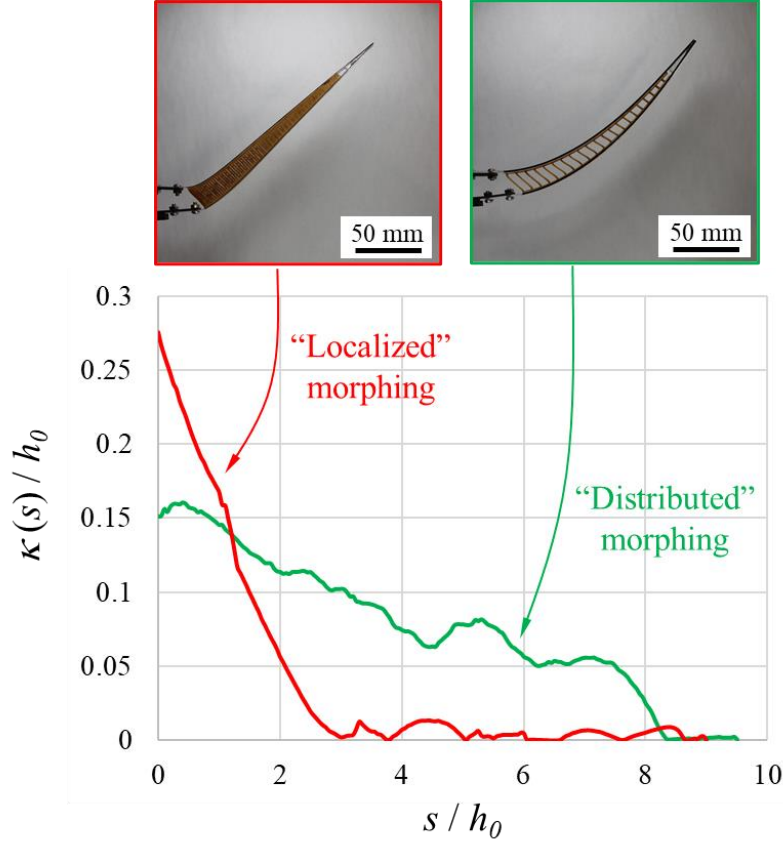
Figure 9: Normalized local curvature as a function of curvilinear position along the ray. The red curve shows an example of "localized morphing" where the deformations are concentrated near the base of the ray, which is not desirable. The green curve is an example of "distributed morphing" where curvature from morphing is better distributed along the length of the ray.

In a recent study on morphing lattice beams [55], we have examined several possible metrics for flexural morphing, all based on curvature. The maximum curvature κ_{max} and an average curvature $\bar{\kappa}$ (the curvature averaged over the length of the ray) were first considered as morphing metrics, but these metrics are not adequate: Cases where the deformations are concentrated near the base of the ray, forming a deformation "hinge" represent poor morphing response but produce high values of these metrics (the very high curvature near the base of the ray biasing κ_{max} and $\bar{\kappa}$ towards high values). A better metric is the first moment of curvature $\kappa^{(1)}$ given by[55]:

$$\kappa^{(1)} = \frac{1}{L}\int_0^L s\kappa(s)ds \qquad (2)$$

15

Large curvatures away from the base of the ray produce $\kappa^{(1)}$ values, and therefore $\kappa^{(1)}$ captures morphing that occurs over long distances along the ray. $\kappa^{(1)}$ is a robust, nondimensional metric of the flexural morphing of the ray in terms of deformations, which can be used to compare and rank different fin designs. Figure 10 shows $\kappa^{(1)}$ as a function of the relative stiffness of the core, obtained from experiments and from the nonlinear finite element model for an actuation distance $u_0 = 13$ mm. The reference is the coreless ray ($E_c = 0$). For the coreless case, buckling of the compressive hemitrich impedes morphing and limits $\kappa^{(1)}$. Both the model and the experiments show a similar trend: The addition of ligaments keeps the hemitrichs together and adds stability, leading to higher values for $\kappa^{(1)}$ ($\kappa^{(1)} \sim 0.2$), but only in the range of relative core thickness $1 < \dfrac{E_c h_0^4}{(EI)_h} < 10$. For

higher relative core stiffness $\dfrac{E_c h_0^4}{(EI)_h} > 10$, $\kappa^{(1)}$ decreases because as the core region becomes too stiff, morphing becomes concentrated near the base. In summary, the ligaments in the core are critical to stabilize the hemitrichs and prevent buckling, but too many ligaments and a high relative core stiffness lead to a hinge-type of response (Figure 9) which is not desired.
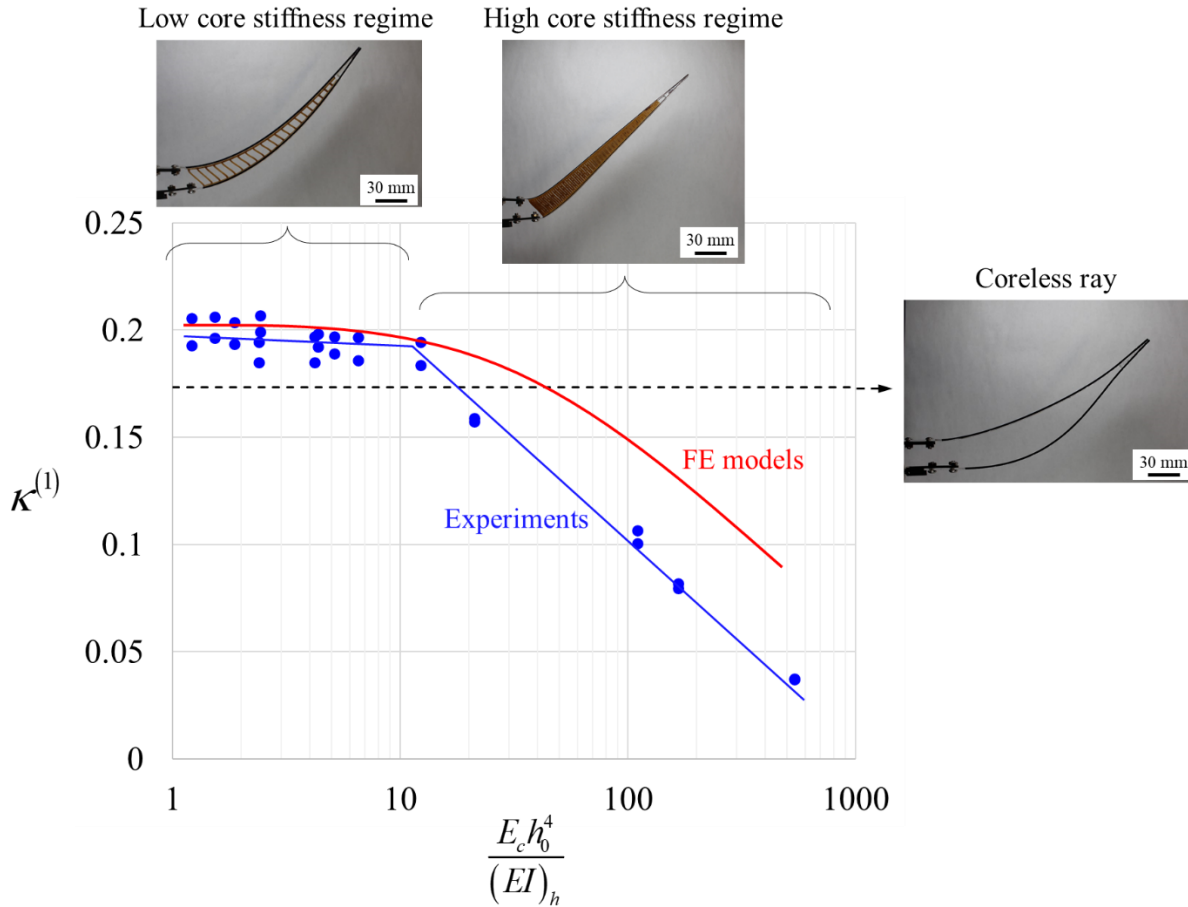
Figure 10: First moment of curvature $\kappa^{(1)}$ as a function of relative core modulus across fin rays with different core spacings. Typical snapshots for the different regimes are also shown.

Morphing compliance: Another metric of interest is the amount of actuation force required to morph the ray. Figure 11a shows a set of representative F_0 - u_0 curves (actuation force as function of actuation distance) for different designs. The coreless designs and the design with rubber ligaments show the same initial morphing stiffness, because at small deformations, the ligaments are mechanically invisible. There are however pronounced differences at higher deformations as non-linear mechanisms become pronounced. In the coreless design, the buckling of one of the hemitrich leads to a softening F_0 - u_0 response. For the design with ligaments, the progressive stretching and large rotations of the ligaments stabilizes the ray but it also leads to a stiffening

response similar to what we observed on the natural ray [27]. As expected, the amount of stiffening

is more pronounced as the ligament density is increased. For comparison we also show the results

from the all-PMMA ray (Figure 3e), which produces a stiff linear response restricted to small

deformations (high deformations broke the ray). To quantitatively compare these designs, we use

the morphing compliance Q to capture the "ease" of morphing the ray from a set of forces at the

base. It is simply written:

$$Q = \frac{u_0}{F_0} \qquad\qquad (3)$$

Where u_0 is the base actuation displacement and F_0 is the actuation force at the base of the ray. By

this metric, the different designs only show differences at large deformations, for which the

response is non-linear. For this reason, we used the secant modulus of the $F_0 - u_0$ curves, taken at

an actuation distance of $u_0 = 13$ mm for all designs. Figure 11b shows the morphing compliance,

normalized by the morphing compliance of the coreless design, as function of relative core

stiffness. Both experiments and FE models show a similar trend: The designs with ligaments are

2.5 to 5 times less compliant than the coreless design (they require 2.5 to 5 times more force to

morph). As expected, the morphing compliance decreases for stiffer relative core stiffnesses.
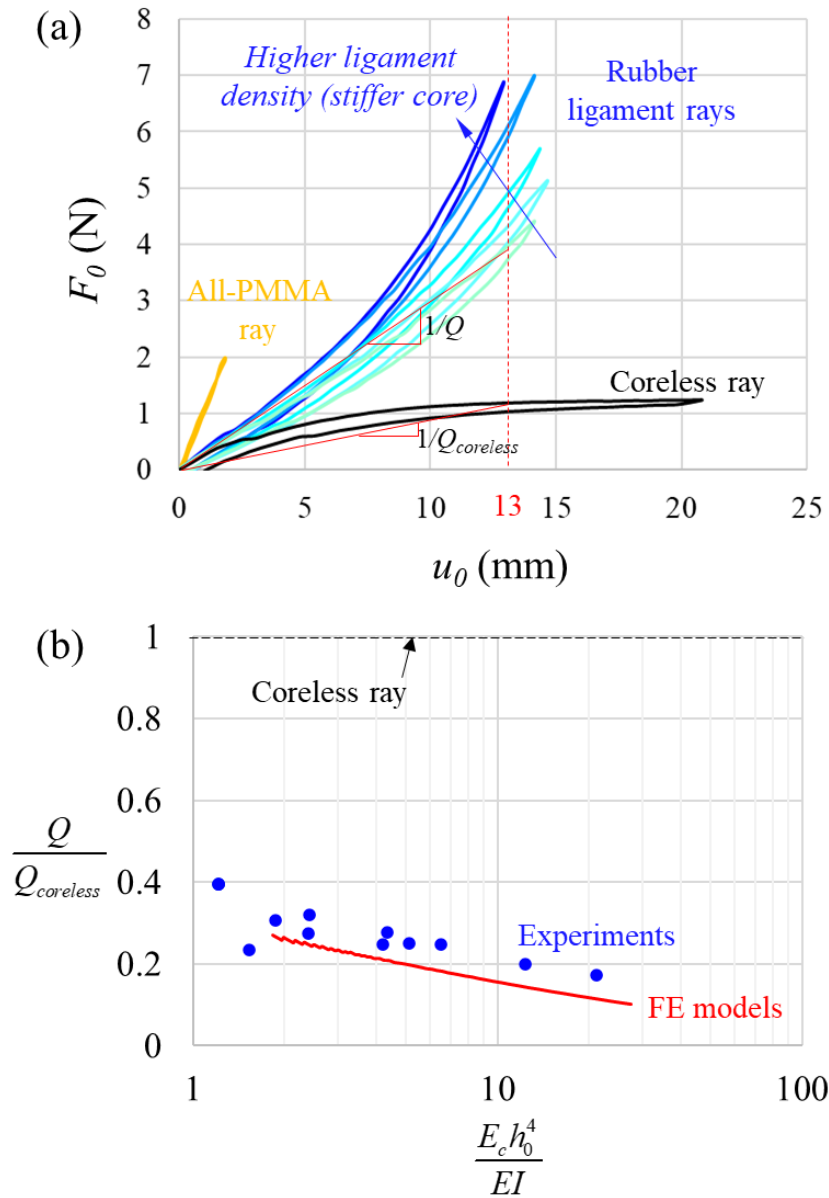
Figure 11: (a) F_0-u_0 curves for different synthetic fin rays. The actuation stiffness increases (and the compliance Q decreases) for stiffer core stiffness E_c. The coreless ray shows softening associated with buckling. (b) Morphing compliance, normalized by the morphing compliance of the coreless design ($E_c = 0$) from models and experiments.

Flexural stiffness: Natural fins can be morphed to large amplitudes, but they also need to be relatively stiff to produce and sustain hydrodynamic forces without collapsing. A third metric we considered for our synthetic rays is flexural stiffness, which we measured as the stiffness of the ray when subjected to a transverse force. Figure 12a shows representative transverse force-deflection curves (*P-δ* curves) for different designs. The coreless design and the rubber ligament designs all show the same initial flexural stiffness, again because the ligaments are mechanically invisible at small deformations. At larger deformations the curves soften because of buckling. However, the results clearly show that buckling can be delayed by increasing the density of the ligaments. An all-PMMA representative *P-δ* curve is also shown, which shows a much stiffer response but which is restricted to small deformations. In order to measure the flexural stiffness of the ray in a way that accounts for large deformation regimes, we used a secant modulus taken at *δ* = 18 mm for all designs. Figure 12b shows the secant flexural stiffness, normalized by the flexural stiffness of the coreless design, as function of the relative stiffness of the core. Even the lowest density of rubber ligament increases the flexural stiffness by about 40%, by delaying buckling and from $\dfrac{E_c h_0^4}{(EI)_h} \approx 2-3$, the flexural stiffness continuously increases with relative core stiffness. The finite element models overestimate the experiments by about 10-20%, but they properly capture the trend of flexural stiffness vs. relative core stiffness.
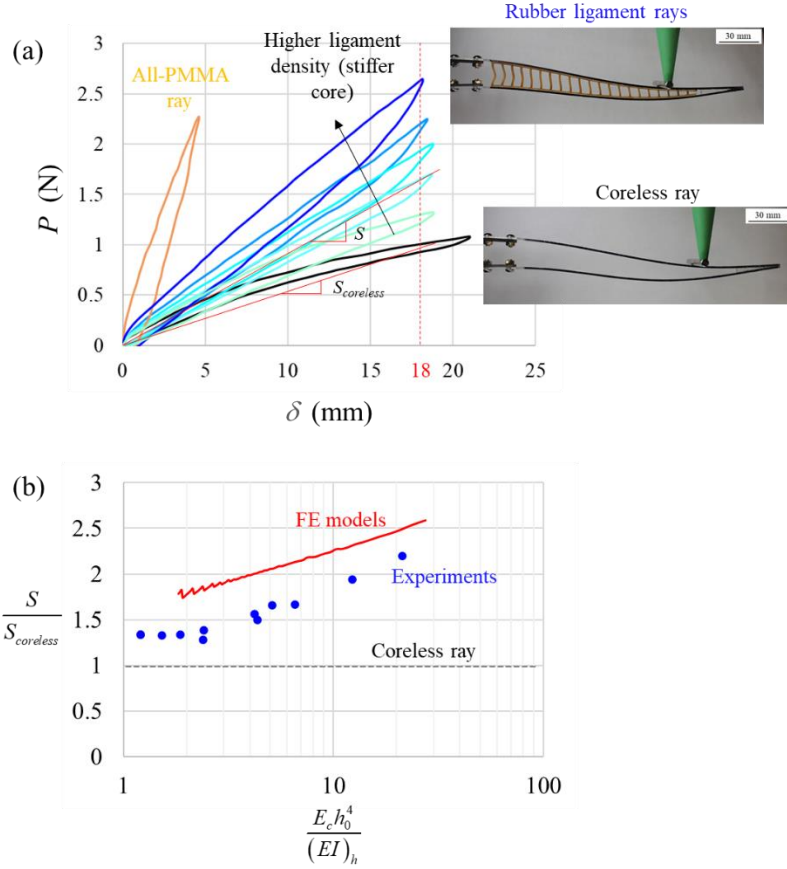
Figure 12: (a) *P-δ* curves for different synthetic fin rays. The secant flexural stiffness increases for stiffer core stiffness E_c. The coreless ray shows softening associated with buckling. (b) Flexural stiffness, normalized by the morphing compliance of the coreless design ($E_c = 0$) from models and experiments.

Multi-objective plots: The ideal ray combines high morphing $\kappa^{(1)}$, high morphing compliance Q and high flexural stiffness S. However, the results above suggest that some of these performance metrics are conflicting. For example, higher ligament densities increase the flexural stiffness, but also decrease the morphing compliance. To visualize these trade-offs, it is useful to plot these metrics on a performance map, which we constructed by considering different possible combinations of core modulus E_r and ligament spacing d in the 1 to 20 mm range for the finite element models. All three metrics were then normalized by the performance of the coreless design to create the map shown on Figure 13. The possible combinations of flexural stiffness and morphing compliance all lie on a narrow region on the map, which is largely governed by the

relative core stiffness parameter $\dfrac{E_c h_0^4}{(EI)_h}$. Closer examination of the model revealed that the

"thickness" of that region is due to the flexural stiffness of the ligaments, which has a much smaller

effect than the relative core stiffness, but which must be accounted for in the model to match the

experiments, especially for designs with larger ligament densities. As expected, the coreless ray

produces the highest morphing compliance, but the lowest flexural stiffness. As the ligaments are

added and their density is increased, $\dfrac{E_c h_0^4}{(EI)_h}$ increases, with the effect of decreasing the morphing

compliance and increasing the flexural stiffness. The map therefore clearly shows the trade-off

between these two properties. On the other hand, the morphing parameter $\kappa^{(1)}$, shown as color-

coded on the map of Figure 13, shows a clear optimum region on the map within the range

$1 < \dfrac{E_c h_0^4}{(EI)_h} < 10$ producing the highest values. The experimental results for various designs, also

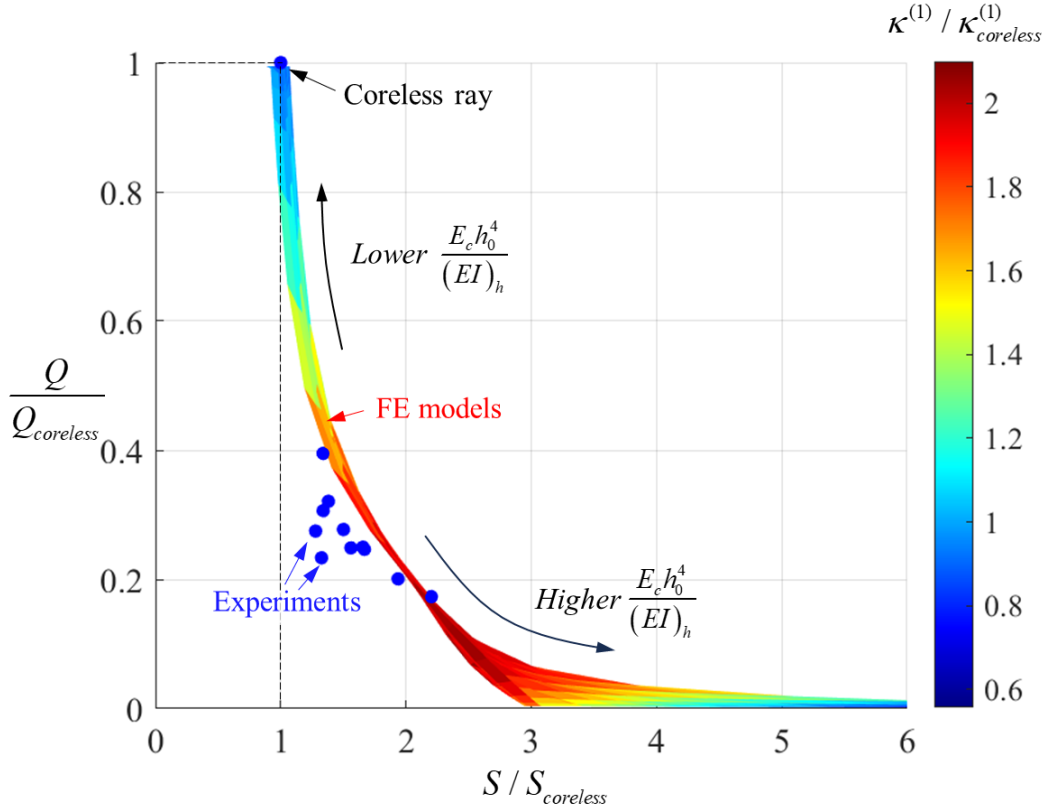shown in Figure 13, agree well with the model.

Figure 13: Performance map showing the morphing compliance Q, the flexural stiffness S and the first moment of curvature $\kappa^{(1)}$, from finite element (FE) models and from experiments. All properties are normalized by the properties of the coreless design.

We finally consider the parameter $C = Q.S$, which must be maximized to combine high morphing compliance and high flexural stiffness, and which is useful to compare fish fins with other morphing materials. The mechanical forces and stiffness are not always fully characterized for other morphing materials, and the values depend greatly on dimensions and configurations. Nevertheless, C can be estimated using simple assumptions and models. We consider here a $L = 200$ mm beam with cross section $h \times h = 400$ mm^2. The flexural stiffness of the beams is then estimated using $S \sim Eh^4 / L^3$, with the modulus E dependent of the material of which the structure is made. The first example we used for comparison is a very soft morphing structure: Pneumatic morphing systems that include inflatable fabrics [56] and pneumatic cells [57]. In these materials

the modulus is the order $E\sim100$ kPa, and the actuation compliance can be estimated using $Q \approx \lambda L / P_a A$ where P_a is the actuation air pressure (typically in the order of 0.1 MPa), A is the cross section of the structure, and λ is the stretch ratio of the pressurized cells (typically $\lambda \sim 1.5$). Using these estimates, we calculated $C = Q.S \sim 10^{-4}$ to 10^{-2} for pneumatic morphing systems. On the opposite end of the stiffness range for morphing materials, we examined stiff structural materials ($E\sim100$ GPa) actuated with piezoelectric shear actuators [58]. For this class of morphing materials, the actuation force can be estimated using EAd_pe, where d_p is the piezoelectric coefficient ($d_p \sim 10^{12}$ mV) and e is the strength of the electric field. Using these assumptions, we estimated $C \sim 10^{-2}$ for piezoelectric-actuated stiff structures. For comparison, our synthetic fins produced $C \sim 10^{-1}$, which we directly calculated using the data of Figure 5 and Figure 6. These estimates suggest that morphing beams inspired from rays provide advantageous combinations of low actuation forces and high flexural stiffness compared to existing morphing technologies.

Conclusions

Fish fins are fascinating structures which are relatively stiff, but which can be morphed from small push-pull forces applied at their base. They can serve as model for improved stiff morphing engineering materials, but further development is slowed by the lack of mechanical models at regimes of large deformations, and by the lack of guidelines for design and optimization. In this study we have designed, fabricated and tested synthetic fin rays that duplicate some of the key features of natural fish fin rays. We used a combination of experiments and nonlinear finite elements models to reach the following main conclusions:

24

- The combination of a very soft material (rubber) with a ligamentous design enables core regions which are 3-4 orders of magnitude more compliant than the hemitrichs.

- The morphing and deformation mechanisms observed on natural fin rays could be duplicated in our synthetic rays.

- The ligamentous architecture in the core region is critical so that the ligaments are "mechanically invisible" at small deformations, which minimizes the force required to initiate morphing.

- The ligamentous design in the core region is critical to stabilize the structure at large deformations, by delaying the buckling of the hemitrichs in both morphing and flexural loading configurations.

- The stiffness of the core region can be easily tuned by changing the spacing between ligaments.

- The ligaments are required to achieve morphing deformations distributed over the entire ray, which we measure using the first moment of curvature. The ligaments provide a constant morphing shape over a wide range of stiffnesses. However, if the stiffness of the core is too high, morphing localizes in a "hinge" near the base of the ray, so that the morphing shape is optimum only for a certain range of stiffness in the core region.

- The main parameter that governs the mechanics and performance of the ray is the ratio between the tensile stiffness of the core and the flexural stiffness of the hemitrichs. The flexural stiffness of the ligament has much smaller effects, but it must be accounted for to match the experiments, especially at high ligament densities.

- A property map showing all three metrics can be used to guide the design of ray-like morphing beams. There is a strong trade-off between morphing compliance (the actuation forces required

to morph the ray) and flexural stiffness, but there is a clear region where the morphing shape is optimum.

While this structure captured some of the main features of natural fin rays, there are many possible extensions and enrichments of the design that could incorporate some finer features inspired from natural fin rays (Figure 1). Segmentations in the hemitrichs could be added to the design to achieve better trade-offs between morphing compliance and flexural stiffness [28]. The section of the hemitrich also decreases towards the end of the rays, which creates a gradient of flexural properties that could also improve the mechanical performance of the rays. Other finer features in natural rays include semi cylindrical three-dimensional bony segments in the hemitrichs, crimps in the collagen fibrils, and non-uniform distributions of ligament spacings. The mechanical role of these features is not fully understood, but the fabrication, testing and modeling platforms we developed here could serve as mechanical models to better understand these more complex structure-property relationships in natural fins. These additional features could also lead to even better stiff morphing bioinspired structures for a variety of applications in aerospace, biomedicine, or robotics.

Acknowledgments

References

[1]   R. M. Ajaj, C. S. Beaverstock, and M. I. Friswell, "Morphing aircraft: The need for a new design philosophy," *Aerospace Science and Technology*, vol. 49, pp. 154–166, Feb. 2016, doi: 10.1016/j.ast.2015.11.039.

[2]   K. Bertoldi, V. Vitelli, J. Christensen, and M. van Hecke, "Flexible mechanical metamaterials," *Nat Rev Mater*, vol. 2, no. 11, Art. no. 11, Oct. 2017, doi: 10.1038/natrevmats.2017.66.

[3]   T. Frenzel, M. Kadic, and M. Wegener, "Three-dimensional mechanical metamaterials with a twist," *Science*, vol. 358, no. 6366, pp. 1072–1074, Nov. 2017, doi: 10.1126/science.aao4640.

[4]   C. Coulais, E. Teomy, K. de Reus, Y. Shokef, and M. van Hecke, "Combinatorial design of textured mechanical metamaterials," *Nature*, vol. 535, no. 7613, Art. no. 7613, Jul. 2016, doi: 10.1038/nature18960.

[5]   P. Celli *et al.*, "Shape-morphing architected sheets with non-periodic cut patterns," *Soft Matter*, vol. 14, no. 48, pp. 9744–9749, Dec. 2018, doi: 10.1039/C8SM02082E.

[6]   D. Restrepo, N. D. Mankame, and P. D. Zavattieri, "Phase transforming cellular materials," *Extreme Mechanics Letters*, vol. 4, pp. 52–60, Sep. 2015, doi: 10.1016/j.eml.2015.08.001.

[7]   E. Hawkes *et al.*, "Programmable matter by folding," *Proceedings of the National Academy of Sciences*, vol. 107, no. 28, pp. 12441–12445, Jul. 2010, doi: 10.1073/pnas.0914069107.

[8]   Y. Cho *et al.*, "Engineering the shape and structure of materials by fractal cut," *Proceedings of the National Academy of Sciences*, vol. 111, no. 49, pp. 17390–17395, Dec. 2014, doi: 10.1073/pnas.1417276111.

[9]   S.-J. Jeon, A. W. Hauser, and R. C. Hayward, "Shape-Morphing Materials from Stimuli-Responsive Hydrogel Hybrids," *Acc. Chem. Res.*, vol. 50, no. 2, pp. 161–169, Feb. 2017, doi: 10.1021/acs.accounts.6b00570.

[10] E. Reyssat and L. Mahadevan, "Hygromorphs: from pine cones to biomimetic bilayers," *J R Soc Interface*, vol. 6, no. 39, pp. 951–957, Oct. 2009, doi: 10.1098/rsif.2009.0184.

[11] E. Siéfert, E. Reyssat, J. Bico, and B. Roman, "Bio-inspired pneumatic shape-morphing elastomers," *Nature Mater*, vol. 18, no. 1, Art. no. 1, Jan. 2019, doi: 10.1038/s41563-018-0219-x.

[12] L. Guiducci, P. Fratzl, Y. J. M. Bréchet, and J. W. C. Dunlop, "Pressurized honeycombs as soft-actuators: a theoretical study," *Journal of The Royal Society Interface*, vol. 11, no. 98, p. 20140458, Sep. 2014, doi: 10.1098/rsif.2014.0458.

[13] A. Benjeddou, "Shear-Mode Piezoceramic Advanced Materials and Structures: A State of the Art," *Mechanics of Advanced Materials and Structures*, vol. 14, no. 4, pp. 263–275, Apr. 2007, doi: 10.1080/15376490600809336.

[14] O. K. Rediniotis, L. N. Wilson, D. C. Lagoudas, and M. M. Khan, "Development of a Shape-Memory-Alloy Actuated Biomimetic Hydrofoil," *Journal of Intelligent Material Systems and Structures*, vol. 13, no. 1, pp. 35–49, Jan. 2002, doi: 10.1177/1045389X02013001534.

[15] C. Thill, J. Etches, I. Bond, K. Potter, and P. Weaver, "Morphing skins," *The Aeronautical Journal*, vol. 112, no. 1129, pp. 117–139, Mar. 2008, doi: 10.1017/S0001924000002062.

[16] K. Maute and G. W. Reich, "Integrated Multidisciplinary Topology Optimization Approach to Adaptive Wing Design," *Journal of Aircraft*, vol. 43, no. 1, pp. 253–263, Jan. 2006, doi: 10.2514/1.12802.

[17] D. M. Boston, F. R. Phillips, T. C. Henry, and A. F. Arrieta, "Spanwise wing morphing using multistable cellular metastructures," *Extreme Mechanics Letters*, vol. 53, p. 101706, May 2022, doi: 10.1016/j.eml.2022.101706.

[18] B. K. Woods, O. Bilgen, and M. I. Friswell, "Wind tunnel testing of the fish bone active camber morphing concept," *Journal of Intelligent Material Systems and Structures*, vol. 25, no. 7, pp. 772–785, May 2014, doi: 10.1177/1045389X14521700.

[19] R. Wu, C. Soutis, S. Zhong, and A. Filippone, "A morphing aerofoil with highly controllable aerodynamic performance," *The Aeronautical Journal*, vol. 121, no. 1235, pp. 54–72, Jan. 2017, doi: 10.1017/aer.2016.113.

[20] B. Jenett *et al.*, "Digital Morphing Wing: Active Wing Shaping Concept Using Composite Lattice-Based Cellular Structures," *Soft Robotics*, vol. 4, no. 1, pp. 33–48, Mar. 2017, doi: 10.1089/soro.2016.0032.

[21] P. Meyer *et al.*, "Transient Dynamic System Behavior of Pressure Actuated Cellular Structures in a Morphing Wing," *Aerospace*, vol. 8, no. 3, Art. no. 3, Mar. 2021, doi: 10.3390/aerospace8030089.

[22] N. B. Cramer *et al.*, "Elastic shape morphing of ultralight structures by programmable assembly," *Smart Mater. Struct.*, vol. 28, no. 5, p. 055006, Apr. 2019, doi: 10.1088/1361-665X/ab0ea2.

[23] J. J. Videler, *Fish Swimming*, 1 online resource (284 pages) vols. Dordrecht: Springer Netherlands, 1993. doi: 10.1007/978-94-011-1580-3.

[24] S. Alben, P. G. Madden, and G. V. Lauder, "The mechanics of active fin-shape control in ray-finned fishes," *Journal of the Royal Society Interface*, vol. 4, no. 13, pp. 243–256, 2007, doi: 10.1098/rsif.2006.0181.

[25] P. J. Geerlink and J. J. Videler, "The Relation Between Structure and Bending Properties of Teleost Fin Rays," *Netherlands Journal of Zoology*, vol. 37, no. 1, p. 59, 1987, doi: 10.1163/002829687X00044.

[26] B. R. Aiello *et al.*, "A comparison of pectoral fin ray morphology and its impact on fin ray flexural stiffness in labriform swimmers," *Journal of Morphology*, vol. 279, no. 8, pp. 1031–1044, 2018, doi: 10.1002/jmor.20830.

[27] S. Das, F. Hannard, and F. Barthelat, "Mechanics and properties of fish fin rays in nonlinear regimes of large deformations," *Acta Biomaterialia*, Jun. 2023, doi: 10.1016/j.actbio.2023.06.029.

[28] F. Hannard, M. Mirkhalaf, A. Ameri, and F. Barthelat, "Segmentations in fins enable large morphing amplitudes combined with high flexural stiffness for fish-inspired robotic

materials," *Science Robotics*, vol. 6, no. 57, p. eabf9710, Aug. 2021, doi: 10.1126/scirobotics.abf9710.

[29] N. K. Taft and B. N. Taft, "Functional implications of morphological specializations among the pectoral fin rays of the benthic longhorn sculpin," *The Journal of Experimental Biology*, vol. 215, no. 15, pp. 2703–2710, 2012, doi: 10.1242/jeb.063958.

[30] C. W. McCutchen, "The trout tail fin: A self-cambering hydrofoil," *Journal of Biomechanics*, vol. 3, no. 3, pp. 271–281, May 1970, doi: 10.1016/0021-9290(70)90029-1.

[31] C. H. White, G. V. Lauder, and H. Bart-Smith, "Tunabot Flex: a tuna-inspired robot with body flexibility improves high-performance swimming," *Bioinspir. Biomim.*, vol. 16, no. 2, p. 026019, Mar. 2021, doi: 10.1088/1748-3190/abb86d.

[32] O. M. Curet, N. A. Patankar, G. V. Lauder, and M. A. MacIver, "Mechanical properties of a bio-inspired robotic knifefish with an undulatory propulsor," *Bioinspir. Biomim.*, vol. 6, no. 2, p. 026004, Apr. 2011, doi: 10.1088/1748-3182/6/2/026004.

[33] C. W. Zhang *et al.*, "Manta Ray Inspired Soft Robot Fish with Tough Hydrogels as Structural Elements," *ACS Appl. Mater. Interfaces*, vol. 14, no. 46, pp. 52430–52439, Nov. 2022, doi: 10.1021/acsami.2c17009.

[34] J. C. Osorio, C. Tinsley, K. Tinsley, and A. F. Arrieta, "Manta Ray inspired multistable soft robot," in *2023 IEEE International Conference on Soft Robotics (RoboSoft)*, Apr. 2023, pp. 1–6. doi: 10.1109/RoboSoft55895.2023.10122038.

[35] Z. Qichao, C. Yingjie, D. Rui, R. Ziyu, T. Wang, and L. Wen, "Bio-inspired flexible robotic caudal fin with three-dimensional locomotion," in *Proceeding of the 11th World Congress on Intelligent Control and Automation*, Jun. 2014, pp. 1881–1886. doi: 10.1109/WCICA.2014.7053007.

[36] S. J. Park *et al.*, "Phototactic guidance of a tissue-engineered soft-robotic ray," *Science*, vol. 353, no. 6295, pp. 158–162, Jul. 2016, doi: 10.1126/science.aaf4292.

[37] W. Coral, C. Rossi, and I. P. Martin, "Bio-inspired morphing caudal fin using shape memory alloy composites for a fish-like robot: Design, fabrication and analysis," in *2015 12th International Conference on Informatics in Control, Automation and Robotics (ICINCO)*, Jul. 2015, pp. 336–343. Accessed: Nov. 24, 2023. [Online]. Available: https://ieeexplore.ieee.org/abstract/document/7347789

[38] T. Hou *et al.*, "Design and Experiments of a Squid-Like Aquatic-Aerial Vehicle with Soft Morphing Fins and Arms," in *2019 International Conference on Robotics and Automation (ICRA)*, May 2019, pp. 4681–4687. doi: 10.1109/ICRA.2019.8793702.

[39] D. Chen, Z. Wu, H. Dong, Y. Meng, and J. Yu, "Platform development and gliding optimization of a robotic flying fish with morphing pectoral fins," *Bioinspir. Biomim.*, vol. 18, no. 3, p. 036010, Apr. 2023, doi: 10.1088/1748-3190/acce86.

[40] L. Li *et al.*, "Aerial-aquatic robots capable of crossing the air-water boundary and hitchhiking on surfaces," *Science Robotics*, vol. 7, no. 66, p. eabm6695, May 2022, doi: 10.1126/scirobotics.abm6695.

[41] M. Bozkurttas, J. Tangorra, G. Lauder, and R. Mittal, "Understanding the Hydrodynamics of Swimming: From Fish Fins to Flexible Propulsors for Autonomous Underwater Vehicles," *Advances in Science and Technology*, vol. 58, pp. 193–202, 2008, doi: 10.4028/www.scientific.net/AST.58.193.

[42] S. Randeni, M. Sacarny, M. Benjamin, and M. Triantafyllou, "Morpheus: An A-sized AUV with morphing fins and algorithms for agile maneuvering." arXiv, Dec. 22, 2022. doi: 10.48550/arXiv.2212.11692.

[43] J. L. Tangorra *et al.*, "The Development of a Biologically Inspired Propulsor for Unmanned Underwater Vehicles," *IEEE Journal of Oceanic Engineering*, vol. 32, no. 3, pp. 533–550, Jul. 2007, doi: 10.1109/JOE.2007.903362.

[44] D. K. Wainwright and G. V. Lauder, "Tunas as a high-performance fish platform for inspiring the next generation of autonomous underwater vehicles," *Bioinspir. Biomim.*, vol. 15, no. 3, p. 035007, Mar. 2020, doi: 10.1088/1748-3190/ab75f7.

[45] S. Randeni, E. M. Mellin, M. Sacarny, S. Cheung, M. Benjamin, and M. Triantafyllou, "Bioinspired morphing fins to provide optimal maneuverability, stability, and response to turbulence in rigid hull AUVs," *Bioinspir. Biomim.*, vol. 17, no. 3, p. 036012, Apr. 2022, doi: 10.1088/1748-3190/ac5a3d.

[46] M. S. Triantafyllou, N. Winey, Y. Trakht, R. Elhassid, and D. Yoerger, "Biomimetic design of dorsal fins for AUVs to enhance maneuverability," *Bioinspir. Biomim.*, vol. 15, no. 3, p. 035003, Mar. 2020, doi: 10.1088/1748-3190/ab6708.

[47] J. L. Tangorra, S. N. Davidson, P. G. Madden, G. V. Lauder, and I. W. Hunter, "A Biorobotic Pectoral Fin for Autonomous Undersea Vehicles," in *2006 International Conference of the IEEE Engineering in Medicine and Biology Society*, Aug. 2006, pp. 2726–2729. doi: 10.1109/IEMBS.2006.260834.

[48] A. P. Mignano, S. Kadapa, J. L. Tangorra, and G. V. Lauder, "Passing the Wake: Using Multiple Fins to Shape Forces for Swimming," *Biomimetics*, vol. 4, no. 1, Art. no. 1, Mar. 2019, doi: 10.3390/biomimetics4010023.

[49] Festo, "BionicTripod with FinGripper." 2009. Accessed: Nov. 28, 2023. [Online]. Available: https://www.festo.com/rep/en_corp/assets/pdf/Tripod_en.pdf

[50] "Micromachines | Free Full-Text | A 3D-Printed Fin Ray Effect Inspired Soft Robotic Gripper with Force Feedback." Accessed: Nov. 05, 2023. [Online]. Available: https://www.mdpi.com/2072-666X/12/10/1141

[51] J. H. Shin, J. G. Park, D. I. Kim, and H. S. Yoon, "A Universal Soft Gripper with the Optimized Fin Ray Finger," *Int. J. of Precis. Eng. and Manuf.-Green Tech.*, vol. 8, no. 3, pp. 889–899, May 2021, doi: 10.1007/s40684-021-00348-1.

[52] W. Crooks, G. Vukasin, M. O'Sullivan, W. Messner, and C. Rogers, "Fin Ray® Effect Inspired Soft Robotic Gripper: From the RoboSoft Grand Challenge toward Optimization," *Frontiers in Robotics and AI*, vol. 3, 2016, Accessed: Nov. 05, 2023. [Online]. Available: https://www.frontiersin.org/articles/10.3389/frobt.2016.00070

[53] "Bio-Inspired Shape-Adaptive Soft Robotic Grippers Augmented with Electroadhesion Functionality | Soft Robotics." Accessed: Nov. 05, 2023. [Online]. Available: https://www.liebertpub.com/doi/10.1089/soro.2018.0120

[54] V. Pratt, "Direct least-squares fitting of algebraic surfaces," in *Proceedings of the 14th annual conference on Computer graphics and interactive techniques*, in SIGGRAPH '87. New York, NY, USA: Association for Computing Machinery, Aug. 1987, pp. 145–152. doi: 10.1145/37401.37420.

[55] K. Yokota and F. Barthelat, "Stiff bioinspired architectured beams bend Saint-Venant's principle and generate large shape morphing," *International Journal of Solids and Structures*, vol. 274, p. 112270, Jul. 2023, doi: 10.1016/j.ijsolstr.2023.112270.

[56] T. Gao, E. Siéfert, A. DeSimone, and B. Roman, "Shape Programming by Modulating Actuation over Hierarchical Length Scales," *Advanced Materials*, vol. 32, no. 47, p. 2004515, 2020, doi: 10.1002/adma.202004515.

[57] T. Gao, J. Bico, and B. Roman, "Pneumatic cells toward absolute Gaussian morphing," *Science*, vol. 381, no. 6660, pp. 862–867, Aug. 2023, doi: 10.1126/science.adi2997.

[58] B. P. Baillargeon and S. S. Vel, "Active Vibration Suppression of Sandwich Beams using Piezoelectric Shear   Actuators: Experiments and Numerical Simulations," *Journal of Intelligent Material Systems and Structures*, vol. 16, no. 6, pp. 517–530, Jun. 2005, doi: 10.1177/1045389X05053154.